

Causes of Long-Term Drought in the U.S. Great Plains

SIEGFRIED D. SCHUBERT, MAX J. SUAREZ, PHILIP J. PEGION,^{*} RANDAL D. KOSTER,
AND JULIO T. BACMEISTER⁺

NASA GSFC, Earth Sciences Directorate, Greenbelt, Maryland

(Manuscript received 12 August 2002, in final form 1 July 2003)

ABSTRACT

The U.S. Great Plains experienced a number of multiyear droughts during the last century, most notably the droughts of the 1930s and 1950s. This study examines the causes of such droughts using ensembles of long-term (1930–2000) simulations carried out with the NASA Seasonal-to-Interannual Prediction Project (NSIPP-1) atmospheric general circulation model (AGCM) forced with observed sea surface temperatures (SSTs). The results show that the model produces long-term (multiyear) variations in precipitation in the Great Plains region (30°–50°N, 95°–105°W) that are similar to those observed.

A correlative analysis suggests that the ensemble-mean low-frequency (time scales longer than about 6 yr) rainfall variations in the Great Plains are linked to a pan-Pacific pattern of SST variability that is the leading empirical orthogonal function (EOF) in the low-frequency SST data. The link between the SST and the Great Plains precipitation is confirmed in idealized AGCM simulations, in which the model is forced by the two polarities of the pan-Pacific SST pattern. The idealized simulations further show that it is primarily the tropical part of the SST anomalies that influences the Great Plains. As such, the Great Plains tend to have above-normal precipitation when the tropical Pacific SSTs are above normal, while there is a tendency for drought when the tropical SSTs are cold. The upper-tropospheric response to the pan-Pacific SST EOF shows a global-scale pattern with a strong wave response in the Pacific and a substantial zonally symmetric component in which U.S. Great Plains pluvial (drought) conditions are associated with reduced (enhanced) heights throughout the extratropics.

The potential predictability of rainfall in the Great Plains associated with SSTs is rather modest, with about one-third of the total low-frequency rainfall variance being forced by SST anomalies. Further idealized experiments with climatological SST suggest that the remaining low-frequency variance in the Great Plains precipitation is the result of interactions with soil moisture. In particular, simulations with soil moisture feedback show a fivefold increase in the variance in annual Great Plains precipitation compared with simulations in which the soil feedback is excluded. In addition to increasing variance, the interactions with the soil introduce a year-to-year memory in the hydrological cycle. The impact of soil memory is consistent with a red noise process, in which the deep soil is forced by white noise and damped with a time scale of about 1.5 yr. As such, the role of low-frequency SST variability is to introduce a bias to the net forcing on the soil moisture that drives the random process preferentially to either wet or dry conditions.

1. Introduction

The U.S. Great Plains experienced a number of major droughts during the last century. The 1930s and 1950s droughts were the most extensive and long lasting. The 1930s drought affected about two-thirds of the country and parts of Canada, though the hardest impacted regions were the central and upper Great Plains (Felch 1978). It was during the 1930s drought that the southern Great Plains, including parts of New Mexico, Texas,

Oklahoma, Colorado, and Kansas, was first characterized as the “Dust Bowl” (Worster 1979)—a reputation it earned from the numerous dust storms that occurred in that region during 1935–37 (Hughes 1976). The 1950s drought was most severe in the southern and central Great Plains. In Texas it was the worst drought on record, with most of the state not having what old timers called “a public rain” for 5 or 6 yr (Hughes 1976). Dust storms were, however, less common than in the 1930s, apparently as a result of weaker winds during this time period (Borchert 1971).

Drought in the Great Plains is not unique to the last century. A number of proxy climate records indicate that multiyear droughts comparable to those of the 1930s and 1950s are, in fact, a regular feature of the Great Plains climate, having occurred approximately once or twice a century over the last 400 years (Woodhouse and Overpeck 1998). Looking still further back

^{*} Additional affiliation: Science Applications International Corporation, Beltsville, Maryland.

⁺ Additional affiliation: Goddard Earth Sciences and Technology Center, University of Maryland, Baltimore, Baltimore, Maryland.

Corresponding author address: Dr. Siegfried D. Schubert, NASA GSFC, Code 910.3, Greenbelt, MD 20771.
E-mail: schubert@dao.gsfc.nasa.gov

in time, there is evidence for multidecadal droughts during the late thirteenth and sixteenth centuries that were of much greater severity and duration than those of the twentieth century (Woodhouse and Overpeck 1998). For example, tree-ring analyses in Nebraska suggest that the drought that began in 1276 lasted 38 years (Bark 1978)!

Considerable research has been done on drought in the Great Plains. Examples include the studies by Namias (1955, 1982), Chang and Wallace (1987), Trenberth et al. (1988), Trenberth and Branstator (1992), Atlas et al. (1993), Lyon and Dole (1995), Beljaars et al. (1996), Trenberth and Guillemot (1996), and Mo et al. (1997). These and other studies have highlighted a number of potentially important factors contributing to dry conditions in the Great Plains, including extratropical and tropical Pacific SST anomalies, soil moisture, changes in the storm tracks, links with the adjacent Pacific and Atlantic anticyclones, and changes in the Great Plains low-level jet. The recent work by Koster et al. (2000) underscores the unique aspects of the Great Plains region that makes it particularly sensitive to changes in soil moisture.

While the above studies have contributed to our understanding of the processes that contribute to drought conditions in the Great Plains, the mechanisms by which a drought can be maintained over many years have not been well established. The extent to which the SST anomalies contributing to drought are tied to the El Niño–Southern Oscillation (ENSO; e.g., Ropelewski and Halpert 1986) would appear to provide one mechanism for multiyear droughts, though the link with ENSO appears to be rather tenuous [except during some major events, e.g., Trenberth et al. (1988)] and would not directly account for decadal droughts such as the one that occurred during the 1930s. In fact the 1930s were marked by a distinct lack of ENSO activity (see, e.g., Fig. 4 in this study). Charney (1975) hypothesized that albedo changes associated with a reduction in vegetation may provide an important feedback mechanism for maintaining droughts in the Sahel. The extent to which vegetation changes are important for maintaining long-term drought in the Great Plains is unknown.

Several studies have examined the nature of long-term drought in the Great Plains. Ting and Wang (1997) show evidence for covariability between U.S. summer precipitation and SST anomalies in the North Pacific Ocean on decadal time scales. Livezey and Smith (1999) show evidence for decadal covariability between U.S. surface temperature and a pan-Pacific SST pattern that encompasses the Tropics and extratropics. Barlow et al. (2001) distinguish between three modes of SST variability that they related to long-term drought in the United States: an ENSO mode, a decadal pan-Pacific mode, and a North Pacific mode. For example, they associated the 1950s (1952–56) drought in the Great Plains with the cold polarity of both the pan-Pacific and the ENSO mode and the 1962–66 drought in the northeastern United States with the North Pacific mode. In this paper we

present an analysis of long-term Great Plains drought in an ensemble of nine 70-yr (1930–2000) simulations carried out with the National Aeronautics and Space Administration (NASA) Seasonal-to-Interannual Prediction Project (NSIPP-1) atmospheric general circulation model (AGCM) forced by observed sea surface temperatures. Our focus is on assessing the causes and predictability of the simulated droughts. Section 2 describes the model simulations and the observations. The results from the 70-yr simulations forced by observed SST are described in section 3. Section 4 presents the results from some idealized SST experiments. Section 5 examines the role of land–atmosphere feedbacks. The discussion and conclusions are given in section 6.

2. The AGCM simulations and observations

The simulations were carried out with the NSIPP-1 AGCM. The model is part of the NSIPP coupled atmosphere–land–ocean model; however, for these experiments, it is run uncoupled from the ocean. The NSIPP-1 AGCM is a gridpoint model. The dynamical core is described in Suarez and Takacs (1995). The boundary layer scheme is a simple K scheme, which calculates turbulent diffusivities for heat and momentum based on Monin–Obukhov similarity theory (Louis et al. 1982). The AGCM uses the relaxed Arakawa–Schubert (RAS) scheme to parameterize convection (Moorthi and Suarez 1992). The parameterization of solar and infrared radiative heating is described in Chou and Suarez (1994, 2000). The mosaic model (Koster and Suarez 1996) is used to represent land processes. Vegetation is prescribed with a climatological seasonal cycle. The simulations described here use a uniform horizontal resolution of 2° latitude by 2.5° longitude and 34 unequally spaced σ layers with high resolution (<200 m) in the lower 2 km of the atmosphere. Details of the NSIPP-1 model formulation and its climate are described in Bacmeister et al. (2000). The seasonal predictability of the model is described in Pegion et al. (2000) for boreal winter, and in Schubert et al. (2002) for boreal summer.

The simulations consist of an ensemble of nine 70-yr (1930–2000) runs forced by observed monthly sea surface temperatures. The runs differ only in their initial atmospheric conditions: these were chosen arbitrarily from previously completed simulations. Since this study was started before the availability of the newest long-term Hadley SST products [the Hadley Centre's Sea Ice and Sea Surface Temperature dataset (HadISST), see later], we used SSTs constructed from three different monthly products. For the period 1930–48 these are an early version of the HadISST product (Rayner et al. 2003). For the period 1949–81 they are the Global Sea Ice and Sea Surface Temperature dataset (GISST) product (Rayner et al. 1996), and for the period 1982–99 they are from Reynolds and Smith (1994). While we attempted to correct for bias in the three SST products, an analysis of our combined SST (hereafter referred to

as the merged SSTs) record nevertheless showed evidence of some minor discontinuities. To reduce the impact of these discontinuities on our results, we have removed from the 70-yr simulations and related observations (as part of the postprocessing steps) the three means (1930–48, 1949–81, 1982–99) separately. This procedure effectively removes long-term trends that may exist in the data.

Another factor that potentially impacts the results is that each model simulation was not carried out as a single continuous run. The runs were instead produced in stages with the first set (seven of the nine ensemble members) of runs starting in December of 1978. The earlier periods were then back-filled, with the second set starting December 1960, and the third set starting in November of 1929. The eighth and ninth ensemble members were started in 1950, and then were back-filled starting in 1929. While these discontinuities should not impact our analysis of the ensemble mean, we are careful to note in the text where calculations (such as filters) involving the individual ensemble members might be impacted.

The model results are compared with a Global Historical Climatology Network (GHCN) 5° latitude–longitude gridded station precipitation dataset available for the period 1900–2001 (Vose et al. 1992). The upper-air fields are compared with the National Centers for Environmental Prediction–National Center for Atmospheric Research (NCEP–NCAR) reanalysis (Kalnay et al. 1996) for the period 1950–2000.

The boreal summer climatology of the NSIPP-1 model is presented in Bacmeister et al. (2000) and is not repeated here. The model does well in reproducing the global distribution of the June–August (JJA) upper-level height and velocity potential fields. In particular, it produces the climatological high over North America with about the correct amplitude and position. The model also does a reasonable job of reproducing the JJA observed global distribution of precipitation, though like many models, it underestimates the precipitation in the eastern Pacific ITCZ, and overestimates the precipitation over the eastern United States. The model also tends to extend high precipitation amounts too far west over the central Great Plains.

3. Drought signal forced by SST

We begin by presenting in this section the results from the nine 70-yr simulations forced by observed SST. The results (simulations and observations) have the three means removed as previously described, and are filtered using a low-frequency filter (Zhang et al. 1997) that retains time scales of about 6 yr and longer. The filter effectively removes ENSO variability allowing us to focus attention on the longer-scale fluctuations such as those that occurred during the 1950s and 1930s. In the following, we refer to this filter simply as the low-fre-

quency filter, and the filtered quantities as low-frequency quantities.

The thin black curves in Fig. 1 denote the low-frequency precipitation from the nine ensemble members averaged over roughly the Great Plains region (30°–50°N, 95°–105°W). The curves are dashed for those time periods where the results are affected by the discontinuities in the simulations as described in section 2. The dashed lines span about 60 months (the length of the low-frequency filter). The heavy solid curve is the low-frequency ensemble mean. The heavy dashed curve is the observed low-frequency rainfall. The results show considerable scatter among the ensemble members though there are clearly time periods during which the curves tend to follow one another. For example, during the 1930s almost all the runs show a tendency for dry conditions, consistent with the observations. This is followed, in the early 1940s, by wet conditions, again consistent with the observations. On the other hand, during the 1950s, the runs show a mixture of dry and wet conditions. Only one of the nine runs is as dry as what was observed. Most of the runs show dry conditions during the mid-1970s, when the observations show a tendency for wet or neutral conditions. During the last two decades almost all the ensemble members show pronounced fluctuations in rainfall that are generally consistent with the observations.

The above results suggest that the model behavior is not inconsistent with the observations in the sense that the observations fall within the spread of the ensemble members. Focusing on the model ensemble results, we see that there are times when the rainfall is potentially predictable if the SSTs are known. In particular, the 1930s drought (with almost all ensemble members showing negative rainfall anomalies throughout much of the decade) appears to have been predictable, but the 1950s drought does not. On average, the contribution of the SST-forced response to the total simulated low-frequency precipitation variance is rather modest over the Great Plains. Table 1 shows the contributions of the signal and noise to the total variance in the Great Plains precipitation for various time scales. The signal is an unbiased estimate of the variance of the ensemble mean (Rowell et al. 1995), and the noise is the estimated intraensemble variance. Here and throughout the text, annual means are computed over a water year (1 October–30 September). This is done to avoid averaging across months in a way that introduces year-to-year correlations that occur due to spring melting of fall snow. For the low frequencies (time scales longer than 6 yr) the signal-to-noise ratio is one-half or, equivalently, the ratio of the ensemble-mean variance to the total low-frequency variance is one-third. For comparison, the signal-to-noise ratio for the annual means is somewhat larger (0.56), while the seasonal means show signal-to-noise ratios that range from 0.12 for boreal winter, to 0.81 for boreal spring. The last column of Table 1 shows that most (two-thirds) of the annual mean precipitation

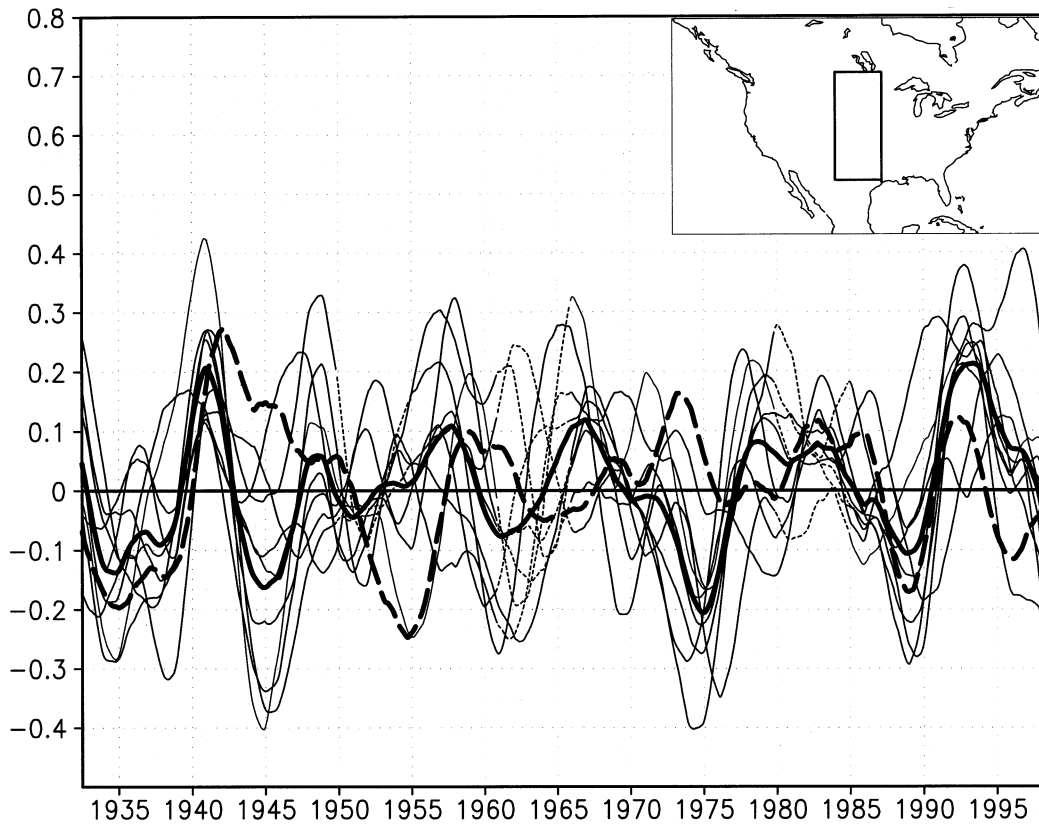


FIG. 1. Time series of precipitation anomalies averaged over the U.S. Great Plains (30° – 50° N, 95° – 105° W, see inset). A filter is applied to remove time scales shorter than about 6 yr. The thin black curves are the results from the nine ensemble members produced with the NSIPP-1 model forced by observed SST. The thin curves are dashed for the time periods where the filter crosses discontinuities in the runs. The thick solid curve is the ensemble mean. The thick dashed curve is the observational estimate. Units are mm day^{-1} .

occurs during spring and summer with approximately equal amounts falling during each season. The remaining one-third of the annual precipitation is divided approximately equally between the other two seasons. The high signal-to-noise ratio together with the relatively large precipitation amounts during spring suggests that this season plays an important role in determining the predictability at annual and longer time scales.

TABLE 1. The precipitation signal variance, noise variance, total variance, signal-to-noise ratio, and the time mean precipitation averaged over the Great Plains (30° – 50° N, 95° – 105° W). Units are in $(\text{mm day}^{-1})^2$ except for the signal-to-noise, which is dimensionless, and the mean precipitation, which is in units of mm day^{-1} . Results are from the nine model simulations for the period 1930–99. The different rows correspond to the four seasonal means, the annual mean, and the low-pass-filtered data (time scales longer than 6 yr).

	Signal	Noise	Total	Signal/ noise	Mean (mm day^{-1})
DJF	0.005	0.045	0.050	0.12	0.97
MAM	0.061	0.076	0.137	0.81	1.95
JJA	0.093	0.338	0.431	0.28	2.16
SON	0.018	0.083	0.101	0.22	0.96
Annual mean	0.026	0.047	0.073	0.56	1.51
Low frequency	0.007	0.015	0.022	0.49	

The relatively large signal-to-noise ratio for spring compared with summer is the result of much smaller noise during the spring season. The reason for the differences in the magnitude of the noise is not clear though it is likely that the spring noise is more “winterlike” in that it is tied to weather systems, while during the summer the noise in the precipitation is associated primarily with small-scale convective systems. The seasonality of the forced response will be discussed further in the next section. Note that the total variance for the different seasons and time scales differs considerably. For example, summer (the rainy season in the Great Plains) has more than 3 times the year-to-year precipitation variance of spring, while the latter has about 3 times the variance of winter. Also, the low frequencies account for only about 30% of the total variance of the annual mean values.

We can obtain some idea of the spatial scale of the simulated Great Plains precipitation fluctuations by correlating the low-frequency ensemble-mean Great Plains precipitation with the low-frequency ensemble-mean precipitation at all other grid points (Fig. 2, top panel). A test based on a Fisher’s Z transform of the correlations (Stuart and Ord 1994) and assuming 15 degrees of free-

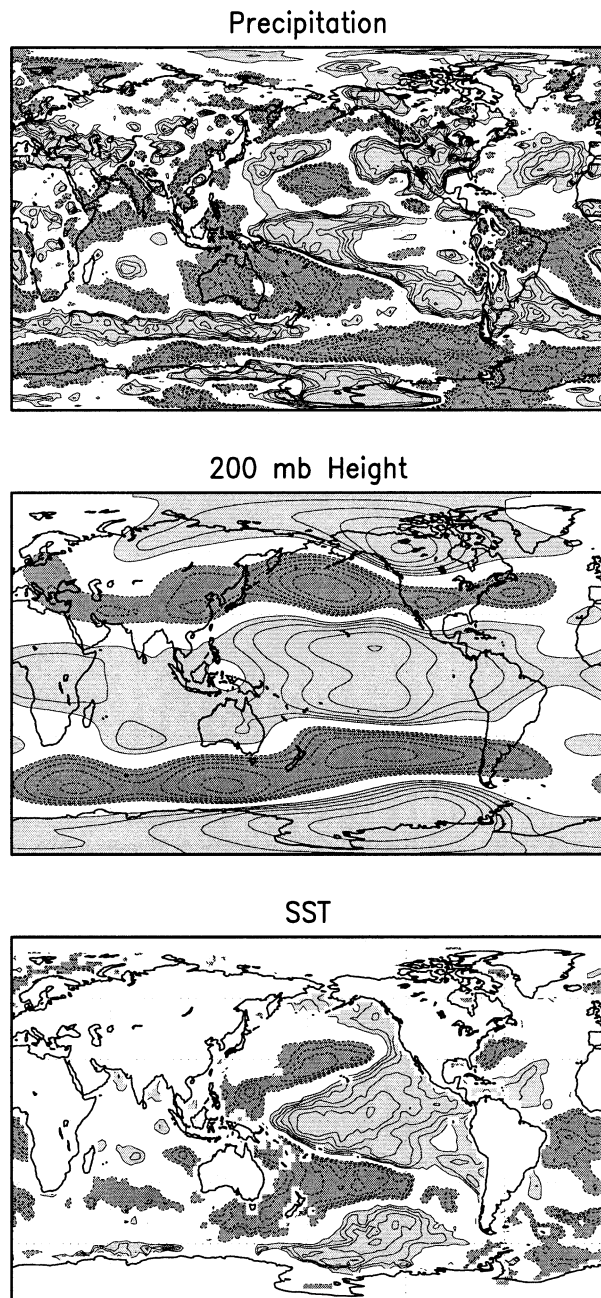


FIG. 2. The correlation between the filtered (time scales greater than 6 yr) ensemble-mean precipitation averaged over the Great Plains (30° – 50° N, 95° – 105° W) and (top) filtered ensemble-mean precipitation everywhere, (middle) filtered ensemble-mean 200-mb height and (bottom) filtered SST for the period 1930–2000. The contour interval is 0.1. The zero and ± 0.1 contours are omitted. Negative correlations have dashed contours and dark shading. Positive correlations have solid contours and light shading.

dom in the filtered time series indicates that absolute values greater than 0.51 are significantly different from 0 at the 5% level. The choice of 15 degrees of freedom assumes a decorrelation time of about 5 yr. This is consistent with the approximate nature of the low-pass filter

that allows some variance to enter at time scales shorter than 6 yr. The correlations show that, in the model, precipitation fluctuations in the Great Plains on long time scales tend to be coherent over much of the continental United States (especially the southern half of the United States and extending into Mexico). Furthermore, the fluctuations have coherence on a global scale, with a tendency for fluctuations of like sign to occur throughout the northern midlatitudes, the southern midlatitudes, and in a region extending from the central tropical Pacific toward southern South America. Fluctuations tend to be of opposite sign to those in the Great Plains in the South Pacific convergence zone (SPCZ), the high-latitude southern oceans, southern Asia, and the tropical Atlantic. The middle panel of Fig. 2 shows the correlations of the low-frequency ensemble-mean Great Plains precipitation with the low-frequency ensemble mean 200-mb height field. The Great Plains precipitation is associated with global-scale height anomalies consisting of a strong wave response emanating from the tropical Pacific into both hemispheres, and a substantial zonally symmetric component. Dry conditions are associated with positive height anomalies in the midlatitudes of both hemispheres and reduced heights in the Tropics and the high latitudes. In general, the height anomalies implied by the correlations appear to be consistent with the tropical precipitation anomalies suggested by the top panel of Fig. 2. For example, wet conditions off the west coast of the United States are associated with an enhanced trough over the North Pacific that would presumably produce more storm systems over the eastern North Pacific.

The correlations between the low-frequency ensemble-mean Great Plains precipitation and the SST (bottom panel of Fig. 2) also show large-scale coherence. Wet conditions in the Great Plains are associated with warm SST anomalies throughout the central tropical Pacific and the North Pacific just off the west coast of North America, warm anomalies over much of the South Pacific, cold anomalies in a “v” shape extending eastward and poleward into both hemispheres from the Pacific warm pool, and cold anomalies in the tropical Atlantic. Zhang et al. (1997), Mantua et al. (1997), and Dettinger et al. (2001) find leading low-frequency SST patterns that are very similar to the SST correlation pattern in Fig. 2, though with larger anomalies in the eastern tropical Pacific. Barlow et al. (2001) find a similar SST pattern as the second leading mode of monthly Pacific SST variability during 1945–93.

It is important to emphasize that the correlation patterns in Fig. 2 are based on ensemble means and individual ensemble members (as well as the observations) do not necessarily produce the same correlation patterns. This is highlighted in Fig. 3 where we show the correlations for eight of the nine ensemble members and the observations. The colored shading in each panel of Fig. 3 displays, over ocean points, the correlations between the Great Plains precipitation and SST and,

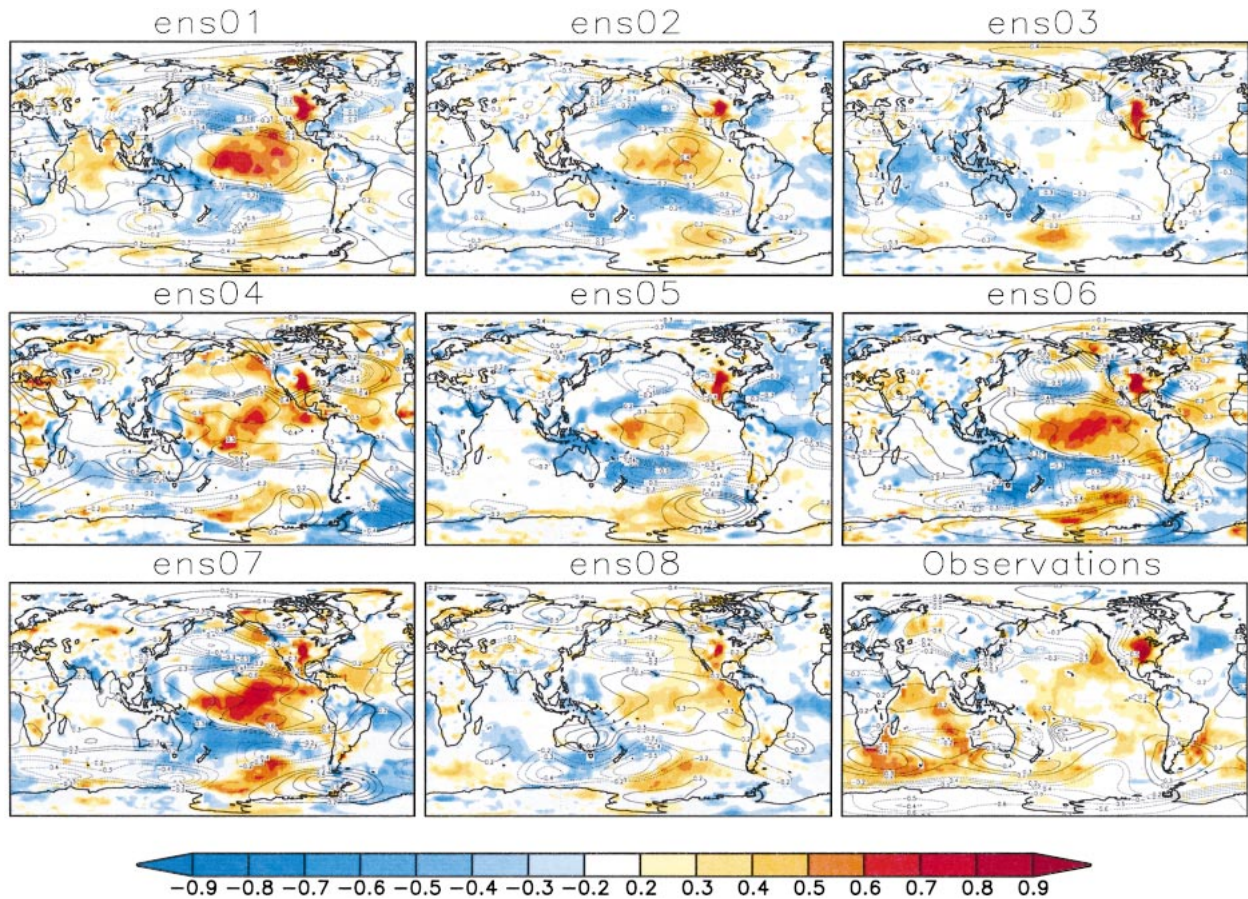


FIG. 3. The color shows the correlations between the filtered (time scales greater than 6 yr) precipitation averaged over the Great Plains and filtered precipitation (over all land points) and filtered SSTs (over all the ocean points). The contours show the correlations between the filtered precipitation averaged over the Great Plains and the filtered 200-mb heights. The contour interval is 0.1. The 0 and ± 0.1 contours are omitted. The negative correlations have dashed contours and the positive correlations have solid contours. The different panels show the results for eight ensemble members and the observations (lower right). Results are based on the period 1930–2000 (1949–2000 for the height observations).

over land points, the correlations between the Great Plains precipitation and precipitation elsewhere. The contours in Fig. 3 show the correlation between Great Plains precipitation and the 200-mb heights. While almost all the ensemble members show some large-scale coherence in the SST correlation patterns (e.g., positive values through the tropical eastern Pacific surrounded by negative correlations to the north and south) there are some ensemble members that show considerably different correlations. Ensemble member 3 shows, for example, overall very weak correlations in the Pacific, while ensemble member 4 shows positive correlations throughout much of the tropical and North Pacific. The results for the observations (lower right panel of Fig. 3) also show a tendency for positive correlations in the eastern Pacific. Perhaps the most notable differences between the model and observational results are the preponderance of positive correlations that occur throughout the Indian Ocean and the Southern Hemisphere for the observations. It is noteworthy that the

Indian Ocean and Southern Hemisphere positive correlations come primarily from the earlier part of the record. In fact, if we compute the correlations between the observed precipitation and SSTs using only the most recent two decades (1979–2000), the correlation pattern is quite similar to that obtained for the ensemble-mean precipitation (bottom panel of Fig. 2).

The correlations between Great Plains precipitation and land precipitation elsewhere (Fig. 3) are generally weak and show considerable intraensemble variability outside the continental United States that is not inconsistent with the observations. The height correlations also exhibit considerable intraensemble variability that is generally consistent with the differences in the SST correlations. Not surprisingly, a number of the height correlation patterns resemble the ensemble mean results shown in Fig. 2b (e.g., ensemble members 1, 6, and 7). Other ensemble members show weaker correlations with the extreme example of ensemble member 3 (top right panel of Fig. 3) showing no evidence of a tropical con-

nection in the height correlations. The latter results are somewhat similar to those for the observations, which also do not show much of a tropical signal in the height correlations (bottom right panel of Fig. 3). The above results serve to highlight the weakness of the link between the SST and the Great Plains precipitation (recall that SST fluctuations account for only about one-third of the Great Plains low-frequency variance) and the fact that individual ensemble members (including the observations) do not provide a good estimate of the relationship between the Great Plains precipitation and the SST.

In order to better establish the link between the SST and the U.S. Great Plains precipitation, we first compute the EOFs (using varimax rotation) of the low-frequency SST for the period 1932–98. The upper-left panel of Fig. 4 shows that the leading EOF has a spatial structure that is very similar to the correlation pattern between the Great Plains and precipitation shown in Fig. 2. We note that rotation has had little effect on the structure of the leading SST EOF—we obtain basically the same EOF without rotation. For comparison with our low-frequency pattern (upper-left panel of Fig. 4), we show in the upper-right panel of Fig. 4 the leading EOF of the residual SST field (total SST – low frequency SST). This pattern is largely confined to the tropical central and eastern Pacific and is clearly related to ENSO (see also the associated time series below).

The time series [principal components (PCs)] corresponding to the above two leading SST EOFs are shown in the middle panel of Fig. 4. The low-pass PC shows substantial negative values during the 1930s, 1950s, and 1970s, indicating from the correlation analysis that those periods should be characterized by dry conditions in the Great Plains. The largest positive values occur in the early 1940s, the late 1950s and 1960s, and the early 1990s, indicating that wet conditions should prevail in the Great Plains during these periods. The residual PC shows large positive values (warm Pacific SST) occurring during 1972/73, 1982/83, 1986/87, and 1997/98, consist with a strong link of this mode to ENSO. There is also a dramatic change in the character of the ENSO signal with much reduced ENSO activity prior to about 1960 (especially during the 1930s). We will discuss the potential implications of that change in ENSO for drought in the Great Plains in the last section. To get some idea of the sensitivity of the leading EOFs to the choice of the SST datasets used, we show in the bottom-left panel of Fig. 4 the leading EOF computed from the HadISST dataset. In this case we do not remove the three separate means (see section 2). The bottom-right panel shows the difference between the two leading EOF patterns. While the two EOFs are generally quite similar, the HadISST EOF does show a more extensive cold (or warm) anomaly pattern in the western Northern Pacific, and more coherent anomalies of the same sign throughout the Tropics, which are part of a warming trend that occurs during this time period (not shown). Further cal-

culations show that the differences in the leading EOF from the two SST datasets shown in Fig. 4 are primarily the result of removing the three separate means from the merged product, and not from any inhomogeneities resulting from the different SST datasets that compose the merged SST data.

We next correlate the leading low-frequency merged SST PC shown in Fig. 4 with the model's ensemble mean low-frequency precipitation at all grid points (top panel of Fig. 5). The pattern is remarkably similar to that produced earlier (top panel of Fig. 2) involving the correlation between the Great Plains precipitation and precipitation at all grid points. This serves to further highlight that the low-frequency ensemble-mean Great Plains precipitation is linked to a dominant global-scale mode of SST variability. For comparison, the lower panel of Fig. 5 shows the correlation between the leading residual (total monthly minus low frequency) SST PC (top-right panel of Fig. 4) with the ensemble-mean residual precipitation. In these calculations, the residuals are based on monthly mean values and a 5-month running mean is applied before computing the correlations. Here, correlations with absolute value greater than 0.36 are significantly different from 0 at the 5% level. The test is again based on Fisher's Z transform of the correlations, though we assume here a decorrelation time of about 2.5 yr (30 degrees of freedom), since the lowest frequencies in the residual ensemble-mean time series are likely dominated by ENSO variability (see middle panel of Fig. 4). Compared with the low-frequency results, the correlations for the residuals have somewhat smaller magnitudes, though the spatial patterns show substantial similarities. The largest differences are in the eastern tropical Pacific and over much of North America. In the eastern tropical Pacific, the residual shows a strong ENSO connection with positive correlations extending all the way to South America and negative anomalies to the north, while the low-frequency results show little correlation in the eastern tropical Pacific. The maximum positive correlations in the tropical Pacific are in somewhat different locations, with the residual correlation maximum located just east of the date line, and the low-frequency correlation located just west of the date line. There are also substantial differences over North America; correlations are strong and positive over much of the continent for the low-frequency results but very weak for the residual calculation.

4. Idealized SST

The above results suggest that low-frequency variations in Great Plains precipitation are, in part, controlled by large-scale pan-Pacific SST anomalies that resemble the leading low-frequency EOF shown in the top-left panel of Fig. 4. We next describe a series of model simulations that are forced with idealized SST anomalies consisting of that leading low-frequency EOF. For

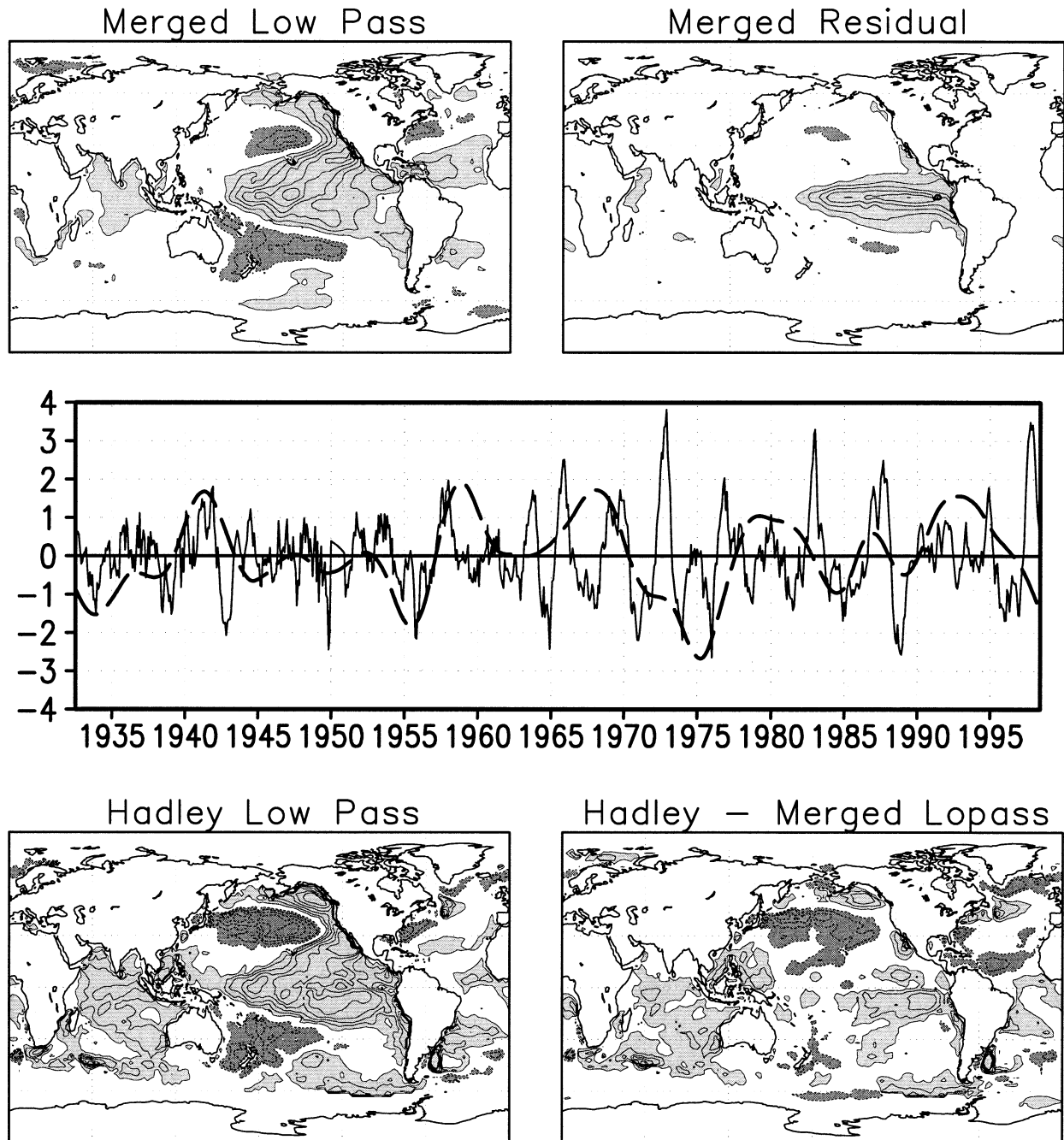


FIG. 4. (top left) The leading EOF of the low-pass-filtered (greater than 6 yr) merged SST for the period 1932–98. (top right) The leading EOF of the residual SST (unfiltered annual mean – low pass). Contour interval is 0.05 (top left) and 0.15 (top right). The zero contour is omitted. Negative values have dashed contours and dark shading. Positive values have solid contours and light shading. (middle) The time series of the PCs of the leading low-pass (heavy dashed curve) and residual (thin solid curve) merged SST EOFs. Units of the PCs are std devs. The product of the PCs and the spatial maps are given in units of $^{\circ}\text{C}$. (bottom left) Same as (top left) but for the HadISST data. (bottom right) The difference between the leading low-pass SST EOFs computed from the merged and HadISSTs.

this purpose, we use the leading low-frequency EOF computed from the HadISST dataset (lower-left panel of Fig. 4). We do this to circumvent the problem of trying to define an SST climatology from the three different SST datasets used in the 70-yr model runs.

Three runs were carried out consisting of two 40-yr simulations that were forced by the two polarities of the low-frequency SST EOF (with an amplitude of two standard deviations) and a third 100-yr run with climatological SSTs (a repeating seasonal cycle). The main pur-

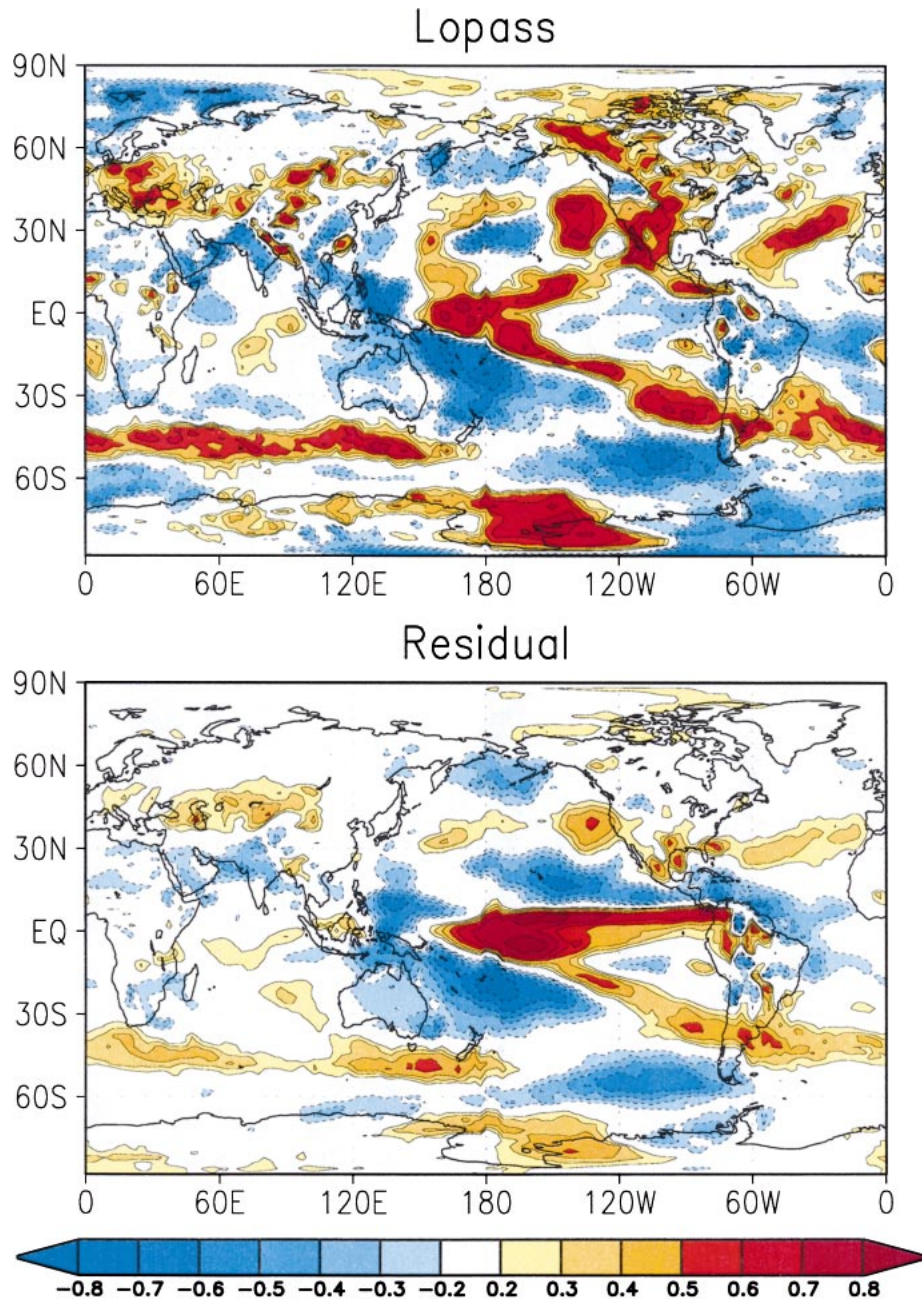


FIG. 5. (top) The correlation between the leading low-frequency merged SST PC and the ensemble-mean low-frequency precipitation for the period 1930–2000. (bottom) The correlation between the leading residual (total – low frequency) merged SST PC and the ensemble-mean residual precipitation for the period 1930–2000. The residuals have a 5-month running mean applied before computing the correlations.

pose of these runs is to verify that the apparent linkages between the Great Plains precipitation and the SST shown in Fig. 2 can indeed be explained as the steady response to a single SST pattern (the pan-Pacific EOF). We are also interested in establishing the linearity of the response to the two polarities of SST EOF. The results for the 200-mb height field are shown in Fig. 6. Here we compare the annual mean anomalies (Decem-

ber–November mean deviations from the climatological run) for the positive and negative polarities of the idealized SST runs (bottom panels), with the analogous fields from the ensemble mean of the original nine 70-yr runs. The latter are computed by compositing the height fields based on the amplitude of the low-frequency pan-Pacific SST EOF in the 70-yr runs. Time periods when the SST EOF is greater than +1 standard

200 mb Height

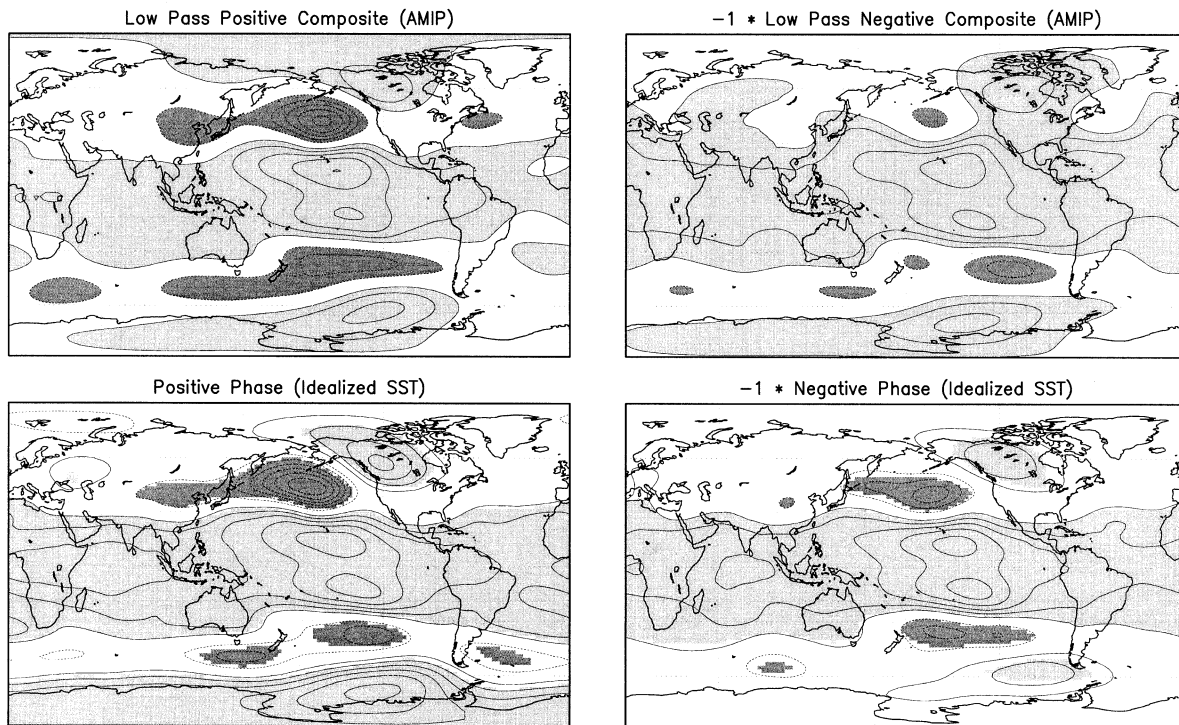


FIG. 6. (top left) Composite 200-mb height anomaly computed from the ensemble-mean low-pass-filtered data. The composite includes all time periods in which the leading low-pass SST EOF (see Fig. 4) has PC values greater than 1 std dev. Values are scaled to be representative of 2 std devs. (top right) Same as (top left) except for when the PC values are less than -1 std devs. (lower left) Annual mean 200-mb height anomaly from the 40-yr run forced with $+2$ std devs in the leading low-pass-filtered SST EOF. (lower right) Annual mean 200-mb height anomaly from the 40-yr run forced with -2 std devs in the leading low-pass-filtered SST EOF. The sign is changed in the right-hand panels to help show any nonlinearities in the response. The contour interval is 5 m and the zero contour is omitted. Only values with absolute values greater than 5 are shaded in the upper panels. In the lower panels all values are shaded, but only where they are significant at the 5% level based on a t test.

deviation contribute to the positive composite, while time periods when the SST EOF is less than -1 standard deviation contribute to the negative composite (upper panels). The composite fields are then scaled to make them representative of a two-standard deviation anomaly. We take this approach (instead of compositing based on two standard deviations in the SST EOF) to obtain more realizations in the composites. We further change the sign of the negative anomalies (right panels) to help identify nonlinearities in the response to the pan-Pacific SST EOF. Comparing the results for the positive polarity and the positive composite (left panels of Fig. 6) shows that the composite anomaly is quite well reproduced by forcing the model with only the low-frequency EOF. There is also considerable similarity between the negative composite and the negative polarity of the idealized run, though in this case there are substantial differences, especially over the North Pacific and North America. This difference appears to be the result of a substantial nonlinearity in the response to the idealized SST. The negative (or cold) polarity of the EOF forcing

produces a generally weaker response in the extratropics compared with the positive (or warm) polarity.

Figure 7 is the same as Fig. 6, except for precipitation. The precipitation also shows generally good agreement between the idealized run and the composite from the 70-yr runs for the positive or warm polarity. The left panels of Fig. 7 both show large positive anomalies in the central tropical Pacific and negative anomalies to the west and to the south. Both also show a tendency for wet conditions over the Great Plains. The negative or cold polarity also shows generally good agreement between the idealized and full SST runs. Both fields show a tendency for dry conditions over the Great Plains. Here there is, surprisingly, less evidence for nonlinearity than for the heights, though there is some tendency for weaker precipitation anomalies in the central tropical Pacific for the negative polarity (cf. bottom panels of Fig. 7). We note that the simulated precipitation anomalies over the Americas are generally consistent with the observational analysis of Dettinger et al. (2001). That study found that the Pacific warm phase

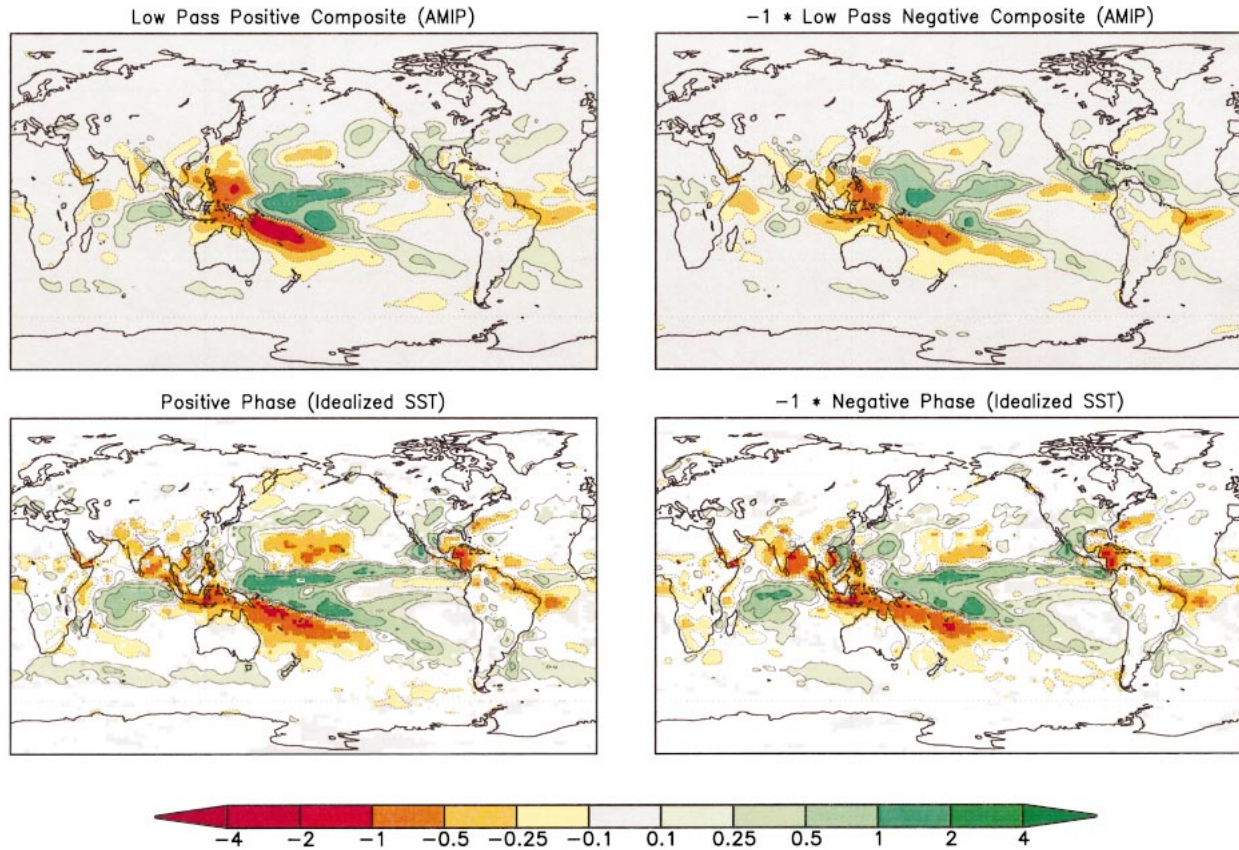


FIG. 7. Same as Fig. 6, except for precipitation. In the lower panels the shading indicates that the values are significant at the 5% level based on a t test. Units are mm day^{-1} .

of the leading pattern of decadal variability in SST (a pattern similar to that shown in the top-left panel of Fig. 4) is associated with enhanced precipitation in the southwestern and central United States, reduced precipitation over northern South America, and enhanced precipitation over parts of central and southern South America, especially near 30°S .

The seasonality of the response to the two polarities of the low-frequency SST EOF is shown in Figs. 8 and 9. We have again changed the sign of the negative anomalies to help identify nonlinearities in the response. The results show a clear seasonal evolution in both the precipitation and 200-mb height response. In the Tropics, the largest seasonal changes in the precipitation response appear to be a tendency toward a north-south split in the anomalies in the eastern Pacific during March-May (MAM) and strong east-west asymmetries in the anomalies during December-February (DJF) with the anomalies of like sign in the Indian Ocean and western Pacific, and anomalies of opposite sign in between. The height field anomalies show a pronounced midlatitude response in the North Pacific-North American region during DJF, while JJA shows a weaker and more zonally symmetric response. Schubert et al. (2002) found a similar tendency for zonal symmetry in the

boreal summer response to SST anomalies that occur on interannual time scales. In general, MAM tends to be more like DJF, while September-November (SON) tends to have many of the characteristics of JJA. A key difference between DJF and MAM occurs for the positive polarity of the SST forcing (cf. left top two panels of Fig. 9). The MAM response shows much more zonally oriented negative anomalies that extend across the southern United States. The zonal extension of the negative height anomalies during MAM is associated with positive precipitation anomalies in the Great Plains (Fig. 8) that are likely due to more storms entering the United States from the Pacific Ocean, and may account for the large differences in the DJF and MAM precipitation signals noted earlier (see Table 1). With the exception of JJA, the Northern Hemisphere shows substantial nonlinearities in the extratropical response (especially cf. left and right top panels of Figs. 8 and 9).

During the positive (wet) polarity of the SST forcing (left panels of Figs. 8-9), the Great Plains precipitation anomalies are largely confined to the spring and summer seasons. The spring anomalies over the Great Plains appear to be associated with a negative height anomaly over the southwestern United States. During the summer the Great Plains precipitation anomalies appear to per-

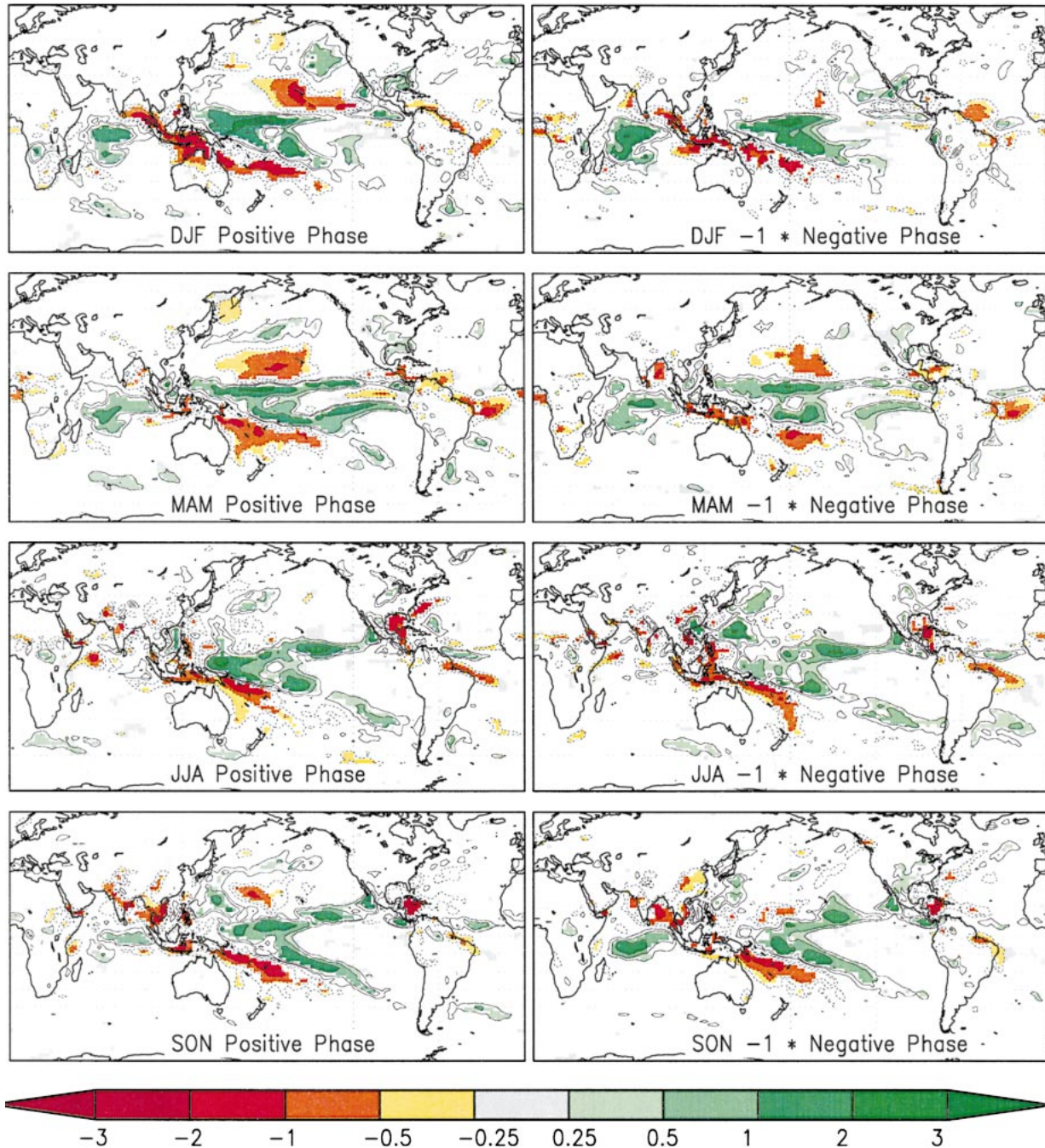


FIG. 8. The seasonal cycle of the response to the idealized SST EOF forcing. (left) The run with +2 std devs in the leading low-pass-filtered SST EOF (right) The run with -2 std devs in the leading low-pass-filtered SST EOF; the sign is changed to help show any nonlinearities in the response. Shading indicates those regions with values significant at the 5% level based on a t test. Units are mm day^{-1} .

sist and/or develop somewhat farther to the north of an anomalous ridge that develops over the south-central United States. During the negative (dry) polarity of the SST forcing (right panels of Figs. 8–9), the Great Plains precipitation anomalies extend from the spring season well into the fall season. The longer-lived Great Plains precipitation anomalies during the negative polarity ap-

pear to be the result of the summerlike zonally symmetric height response (with positive height anomalies over the United States) that lasts into the fall season. This is in contrast to the positive polarity of the SST forcing under which the fall season (SON) shows a substantial seasonal change to an extratropical wave response over the United States that apparently counter-

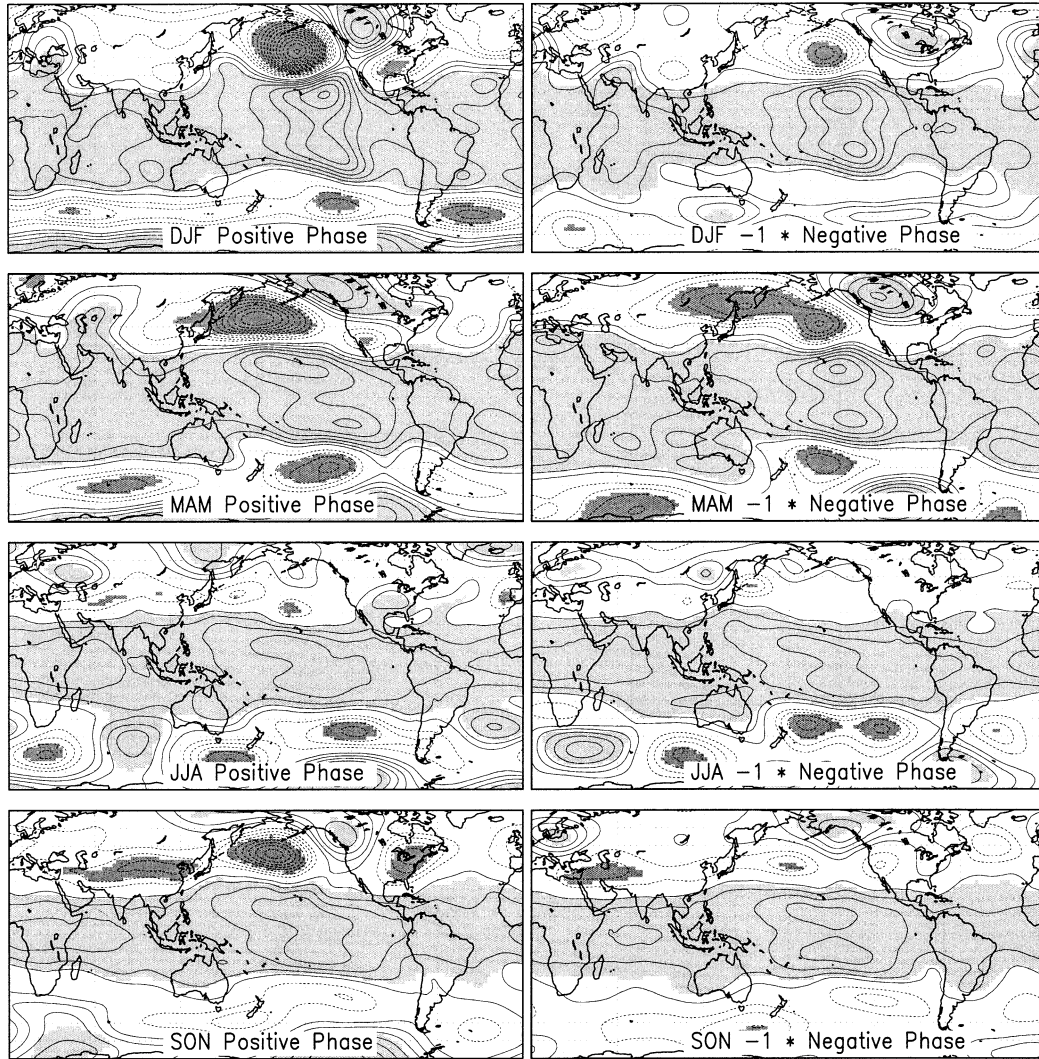


FIG. 9. Same as Fig. 8, except for the 200-mb height field. Contour interval is 5 m and the zero contour is omitted. Negative values have dashed contours and dark shading. Positive values have solid contours and light shading. Shading indicates those regions with values significant at the 5% level based on a t test.

acts the warm season wet conditions (lower-left panel of Fig. 9).

To help assess the relative roles of the tropical and extratropical SST anomalies in the above idealized SST runs, we have carried out further experiments in which the pan-Pacific EOF SST forcing is confined to the Tropics (within $\pm 20^\circ$ latitude). The results of those experiments are very similar to those shown in the bottom panels of Figs. 6 and 7, implying that the tropical SST dominate the response. In Fig. 10 we highlight the impact of the tropical SST on the Great Plains, by showing the temporal evolution of the precipitation in the Great Plains for the runs with the full (top panel) and tropical (bottom panel) EOF SST forcing. The three curves are for the positive SST EOF, negative SST EOF, and climate SST runs. The results show clearly that the positive (warm) polarity produces a tendency for wet conditions

while the cold polarity produces dry conditions. The case with climatological SST tends to fall in between, although it is interesting to note that the run with climatological SST exhibits substantial variability such that at times it is as wet as the warm case (e.g., the first 8 and last 10 yr), while at other times it is as dry as the cold case. We will return to an investigation of the climatological run in the next section. The bottom panel of Fig. 10 shows that the tropical SST results are very similar to those with the full EOF forcing, indicating that the main impact on the Great Plains precipitation comes from the tropical SST anomalies. The straight lines in Fig. 10 denote the time-mean values of the Great Plains precipitation for the positive SST EOF, negative SST EOF, and climate SST runs. The mean values are all significantly different from each other (positive minus negative SST, positive minus climate SST, and neg-

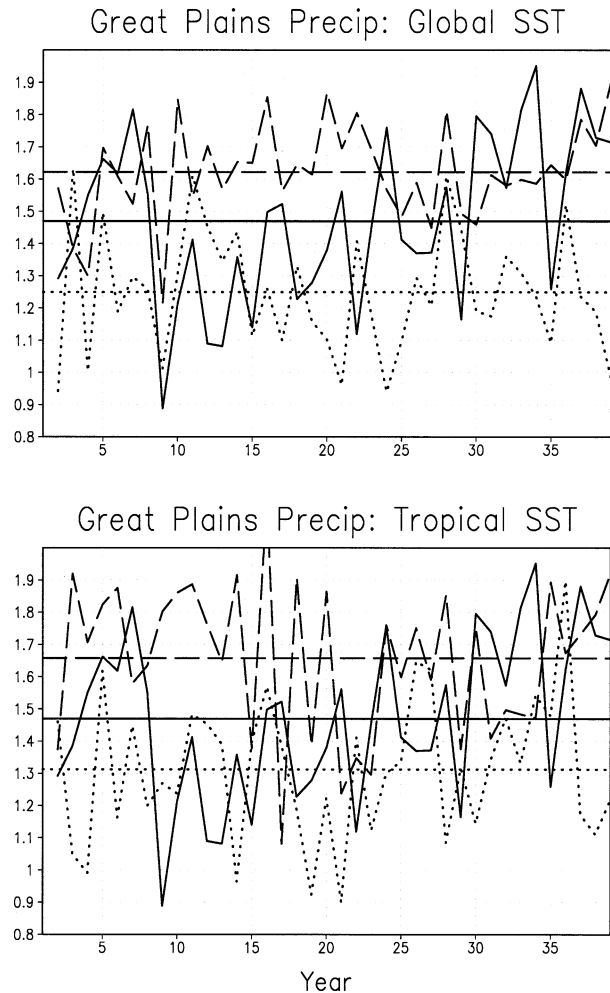


FIG. 10. (top) Time series of the annual mean precipitation over the Great Plains (30° – 50° N, 95° – 105° W) from the runs forced with the leading low-pass-filtered SST EOF (lower-left panel of Fig. 4). The dashed curve is for the run forced with +2 std devs in the EOF. The dotted curve is for the run forced with –2 std devs in the EOF. The solid curve is the control run using climatological SSTs. The straight lines are the corresponding time means. The SST climatology and the EOFs used in the runs were computed from the HADISST data for the period 1930–2000. (bottom) Same as (top) except that the SST anomalies are set to zero poleward of 20° latitude. Units are mm day^{-1} .

ative minus climate SST) at the 5% level based on a t test and assuming the anomalies are independent from one year to the next. In the next section we shall, however, determine that some year-to-year memory occurs in the precipitation even in the absence of anomalous SSTs.

5. Land–atmosphere feedbacks

In this section, we examine the nature of what appear to be decadal fluctuations in Great Plains precipitation that occur even in the absence of time-varying anomalous SST forcing (top panel of Fig. 10), with a partic-

ular focus on the role of soil moisture feedbacks. To facilitate the analysis and to help reduce the sampling errors in the autocorrelation estimates, we have extended the run with climatological SSTs (referred to hereafter as the control run) for another 100 yr for a total of 200 yr. We start by comparing in Fig. 11 the first 100 yr of the control run with a new 100-yr run (described below) in which all feedbacks between the atmosphere and the soil wetness are turned off.

The top-left panel of Fig. 11 shows the time history of the annual mean precipitation (P), evaporation (E), and deep soil wetness (w) in the run with climatological SST. The precipitation fluctuations are similar in magnitude to those from the 70-yr runs shown in Fig. 1. In fact the variance of the annual mean Great Plains precipitation in the control run is about two-thirds that of the 70-yr runs (0.051 versus 0.073; see Tables 1 and 2), consistent with our results from section 3, that showed the SST-forced response accounts for about one-third of the annual mean precipitation variance in the Great Plains. All three quantities (P , E , w) exhibit highly correlated long-term fluctuations. The strong correlation between P and E (0.97) implies that on interannual time scales w fluctuations result from a small residual in a nearly equilibrated surface water budget.

In order to examine the role of soil moisture variations in producing the long-term variations in precipitation shown in the top-left panel of Fig. 11, we carried out a 100-yr simulation in which the effect of the soil moisture feedback is turned off. We do this by fixing the evaporation efficiency or “ β ” (ratio of the evaporation to the potential evaporation) in the land surface model formulation to its seasonal climatology, as described in Koster et al. (2000). Here the potential evaporation is the maximum rate at which the atmosphere can receive water (as controlled by near-surface humidity gradients, wind speed, etc.). The specified values are interpolated between climatological monthly mean β values obtained from a 10-yr segment of the control run. The top-right panel of Fig. 11 shows that the evaporation and more importantly the precipitation variations over the Great Plains are considerably reduced compared with the control run. In fact, we see from Table 2 that the precipitation variance is reduced by a factor of 5, and the evaporation variance is reduced by a factor of 20 compared with the control run [both ratios are significant at the 5% level based on an f test with 200 (100 for the fixed β run) degrees of freedom]. We assume for the purposes of the test that the year-to-year fluctuations are independent though as we shall see, that assumption is violated for the control run. Nevertheless, even a substantially smaller number of degrees of freedom would not change the significance of the results. The reduction in variance is qualitatively consistent with the results of Koster et al. (2000). There are also large differences in the covariances between P and E . As already mentioned, P and E are highly correlated in the control run. In contrast, P and E have a negative correlation (-0.4) in

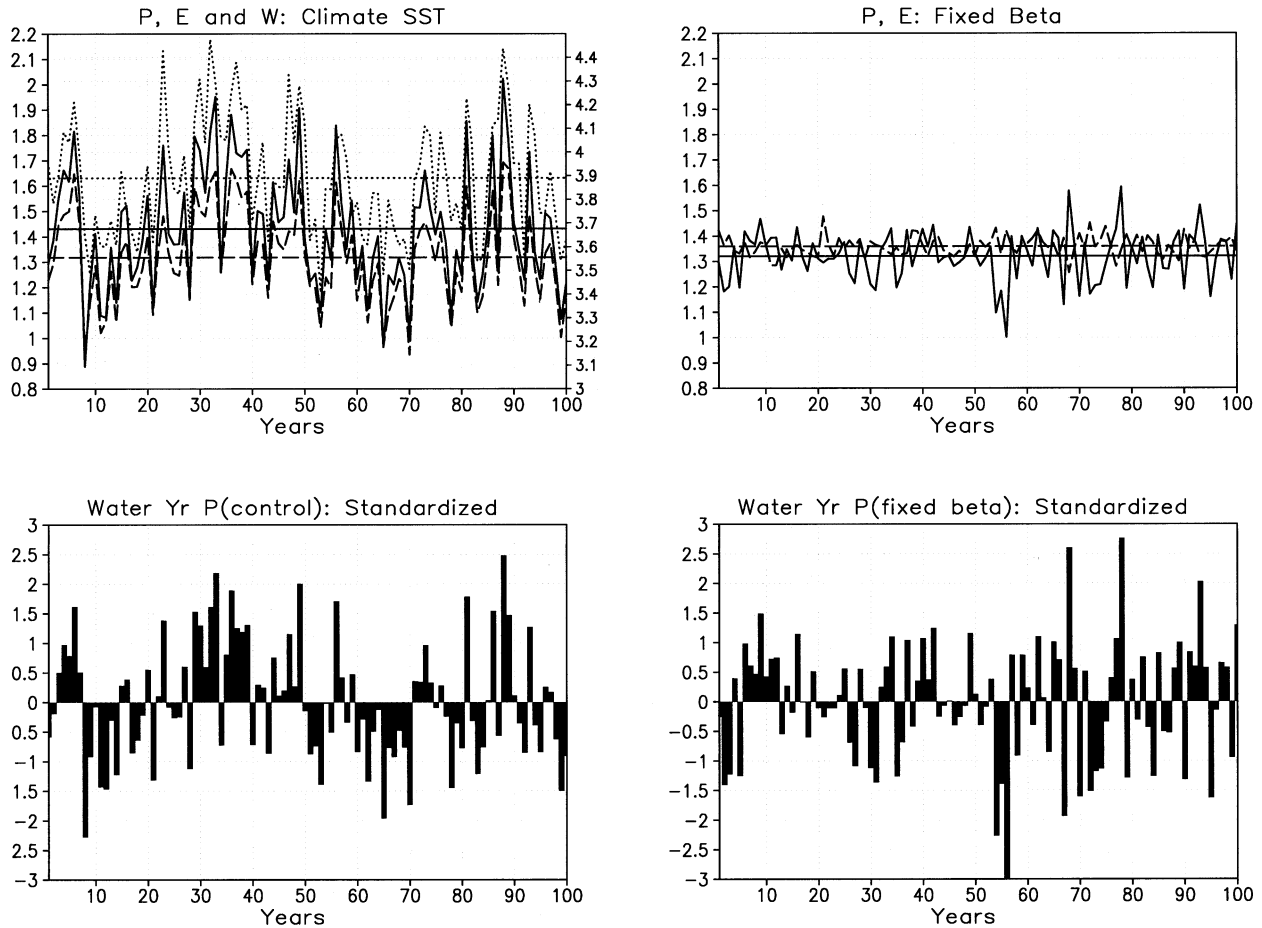


FIG. 11. (top left) Time series of the annual (water year) mean precipitation (solid curve), evaporation (dashed curve), and w (deep soil moisture, dotted curve) over the Great Plains (30° – 50° N, 95° – 105° W), from the control run with climatological SSTs. (top right) Same as (top left) except for the run with climatological SST and fixed β (ratio of the evaporation to the potential evaporation). Note that the soil moisture (w) plays no role in the fixed β run. The units for precipitation and evaporation are mm day^{-1} (left ordinate), and they are dimensionless (values range from 0 to 10) for w (right ordinate). (bottom) The annual mean precipitation from the (left) control run and (right) fixed β run standardized to have zero mean and unit variance.

the fixed β run. This negative correlation may seem surprising if we expect precipitation to respond with like sign to evaporation anomalies, as must be the case in the control run. In the fixed β run, P may indeed be responding positively to E , but the correlation is dominated by the fact that evaporation fluctuations are due almost entirely to fluctuations in the radiative forcing at the surface and these, in turn, are negatively corre-

lated with P (more precipitation/clouds \rightarrow less insolation \rightarrow less evaporation).

The bottom panels of Fig. 11 provide another view of the differences in the Great Plains precipitation in the fixed β and control runs. By normalizing the precipitation to have unit variance and zero mean, we see more clearly that, in addition to impacting the amplitude of the rainfall variations, the interaction with soil mois-

TABLE 2. Lag-1 autocorrelations and variance of annual averages where the annual mean is computed over a water year (1 Oct–30 Sep). Correlations with magnitudes greater than 0.16 are significant at the 5% level (see text). The variance of the deep soil wetness is dimensionless. The other variances have units of $(\text{mm day}^{-1})^2$.

	Control run (200 yr)		Fixed β run (100 yr)	
	Lag-1 autocorrelation	Variance	Lag-1 autocorrelation	Variance
Precipitation (P)	0.12	0.051	−0.02	0.01
Evaporation (E)	0.23	0.030	−0.01	0.0015
Deep soil wetness (w)	0.35	0.0005	—	—

ture appears to also introduce longer time scales into the precipitation variations. Note for example, the 11-yr period (years 61–71) of the control run with consistently negative precipitation (as well as deep soil wetness) anomalies. Also, the extended period of positive precipitation anomalies during years 30–40 is associated with an 11-yr run of positive deep soil moisture anomalies. The probability of such strings of positive or negative values would be rather small if the year-to-year fluctuations in soil moisture were independent. For example, the probability that a given negative value is followed by 10 or more consecutive negative values is equal to 0.001 (assuming equal probability of a positive or negative value).

As already mentioned, we have continued the control run for another 100 yr to help ensure reliable estimates of the autocorrelations in the hydrological cycle parameters. The estimates of the lag-1 autocorrelations are presented in Table 2. To assess the statistical significance of the lag correlations, we generated 10 000 cases of 200 (100 for the fixed β run) independent realizations of a normal random variable with zero mean and unit variance. Each case was treated as a time series of 200 (100) realizations and lag correlations were computed in the same way as for the model output. The 10 000 values were then ordered from smallest to largest and the 9501th (+0.11 for 200 realizations, and +0.16 for 100 realizations) value was taken as the upper 5% significance level. The lag-1 autocorrelations for the fixed β run are all insignificant, indicating that without land feedbacks the annual mean evaporation and precipitation variations are white noise processes. For the control run, all quantities show significant lag-1 autocorrelations, though the precipitation autocorrelation is small with a value of 0.12. The deep soil (w) shows the greatest year-to-year memory with a lag-1 autocorrelation of 0.35, and a lag-2 autocorrelation of 0.15.

An inspection of the time series of the deep soil wetness for the full 200 yr of the control run shows what appear to be long-term changes in the Great Plains deep soil memory. For example, the lag-1 autocorrelation in the deep soil moisture computed from 50-yr segments of the 200-yr run are 0.48, 0.37, -0.02 , and 0.29. While the estimates vary considerably (ranging between zero in the third segment and one-half in the first segment), the differences are not inconsistent with the sampling variations one might expect. For example, assuming a value of 0.35 for the true lag-1 autocorrelation and using Monte Carlo methods to simulate a first-order autoregressive process (see, e.g., Box and Jenkins 1976; see also below), we obtain a probability of 7% for obtaining lag-1 autocorrelations with absolute values that are less than 0.1 from a sample of 50 yr. That leads to a probability of about $1/4$ ($=1 - 0.93^4$) of obtaining at least one sample in four that produces an estimated lag one autocorrelation with absolute values less than 0.1. This illustrates the need for very long simulations to obtain reliable estimates of the memory in the deep soil, and

the difficulty of trying to estimate this quantity from very limited observations.

We can obtain another estimate of the soil memory from the nine-member ensemble of 70-yr runs forced with observed SST. The calculation is done by first removing the ensemble mean from each ensemble member and then computing the ensemble average autocovariance and variance statistics of the deviations. The results obtained from those calculations gives a value of 0.34 for the yearly lag-1 autocorrelation in the deep soil wetness, consistent with the value obtained from the 200-yr climate run. Results for individual ensemble members range from a minimum of 0.17 to a maximum of 0.71 for the lag-1 yr autocorrelation in the deep soil moisture.

The autocorrelation of the deep soil is consistent with a first-order autoregressive (AR 1) process:

$$w(n + 1) = \alpha w(n) + \varepsilon(n). \quad (1)$$

Here n indexes the year, α is the memory parameter in the AR 1 process, and ε is a Gaussian white noise process with zero mean and variance σ_ε^2 . A fit of (1) to the Great Plains annual mean deep soil wetness (w) from the control run gives estimates of $\alpha = 0.35$ (significant at the 1% level) and $\sigma_\varepsilon^2 = 0.00045$. To aid in the interpretation of these results we rewrite (1) as

$$w(n + 1) - w(n) = -(1 - \alpha)w(n) + \varepsilon(n). \quad (2)$$

In this form, we see that the change in the deep soil from one year to the next [the left-hand side of (2)] is due to the white noise forcing (ε) and a damping term. In fact, the changes come primarily from the white noise term, which accounts for about two-thirds of the variance in the year-to-year changes in the deep soil. Statistical stationarity in the deep soil fluctuations is maintained through the damping term [first term on the right-hand side of (2)], which operates on a time scale of $1/(1 - \alpha) = 1.5$ yr. We can associate the damping term with the fraction of the soil moisture forcing (E , P , and runoff) that is implicitly a function of the soil wetness. The white noise term (ε), on the other hand, is likely a statistical residual (on interannual time scales), which is dominated by precipitation fluctuations that are associated with “fast” atmospheric processes such as weather and other convective systems.

While we have so far focused on the local properties of the hydrology over the Great Plains, it is also possible that the local variations are associated with continental and larger-scale atmospheric fluctuations, even in the absence of SST anomalies. Figure 12 shows the correlations between the annual mean Great Plains precipitation and the global distribution of the 200-mb heights (top panel) and the precipitation fields (bottom panel) for the control run. In contrast to the results for the runs with SST anomalies, the correlations in this case show a more local wave train in the 200-mb heights and precipitation (cf. Fig. 2) that extends from Alaska south-eastward across North America and into the Atlantic.

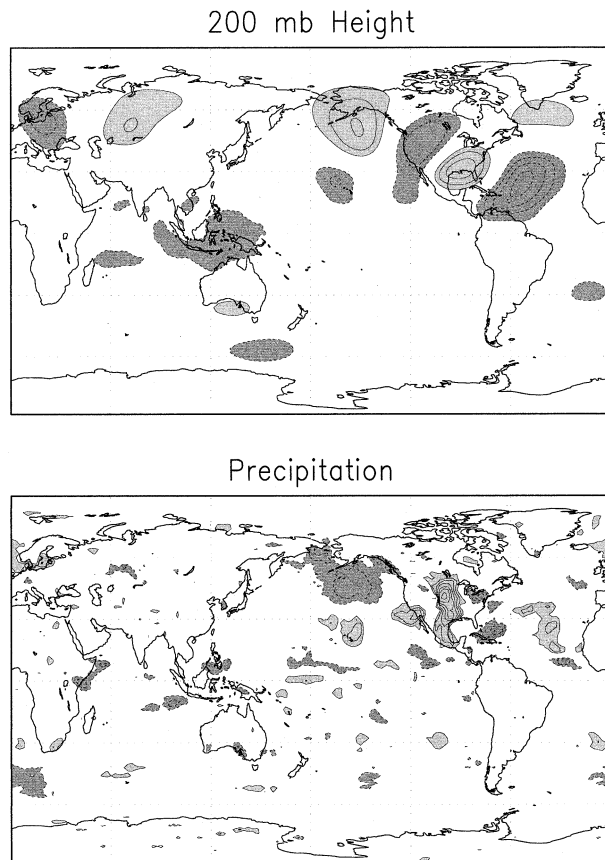


FIG. 12. The correlation between the annual mean precipitation anomalies over the Great Plains and (top) 200-mb height and (bottom) precipitation for the 200-yr control run with climatological SST. The contour interval is 0.1. The zero and ± 0.1 contours are omitted. Negative correlations have dashed contours and dark shading. Positive correlations have solid contours and light shading. Correlations with absolute value greater than 0.14 are significant at the 5% level using the Fisher's Z transform and assuming 200 degrees of freedom.

Separate calculations for DJF and JJA (not shown) indicate that the wave train occurs primarily during boreal winter, while during boreal summer the correlation with height and precipitation is very localized. There is some evidence for correlations with the heights well away from the local response, over Indonesia and Asia, though these are only marginally significant (absolute values must exceed 0.14 to be locally significant at the 5% level using the Fisher's Z transform and assuming 200 degrees of freedom). We have also recomputed the correlations shown in Fig. 12 for the fixed β run. The results (not shown) are generally quite similar, though most of the remote correlations between the Great Plains and the heights are absent.

6. Discussion and conclusions

The results of this study show that the NSIPP-1 model, when forced by observed SSTs, produces low-frequency (multiyear) variations in the U.S. Great Plains

precipitation that are generally consistent with observations. In particular, the model produces the dry conditions of the 1930s "Dust Bowl" era. On the other hand, the model does not show a strong tendency for the dry conditions that were observed during the early 1950s (only one of the nine ensemble members reproduced the dry conditions). A correlative analysis suggests that the low-frequency variations (time scales longer than about 6 yr) in the Great Plains precipitation are linked to variations in a pan-Pacific decadal SST pattern, which is similar to patterns found in previous observational studies (e.g., Zhang et al. 1997; Mantua et al. 1997; Barlow et al. 2001). This connection was confirmed by further AGCM simulations, in which the model was forced by the two polarities of the Pacific SST pattern. The idealized SST simulations further show that it is primarily the tropical part of the SST anomalies that influences the Great Plains. As such, the Great Plains tend to have above-normal precipitation when the tropical SSTs associated with the pan-Pacific pattern are above normal, while there is a tendency for drought when the tropical SSTs are cold. The upper-tropospheric response to the pan-Pacific SST pattern shows a well-defined global-scale pattern with a strong wave response emanating from the tropical Pacific Ocean, and a substantial zonally symmetric component in which Great Plains pluvial (drought) conditions are associated with reduced (enhanced) heights throughout the extratropics. For comparison, on interannual time scales, the ENSO SST anomalies are also positively correlated with precipitation in the Great Plains, but the correlations are much weaker and confined to the southern Plains. Furthermore, the response of the upper-tropospheric height field to boreal summer ENSO SST anomalies shows a substantial zonally symmetric component (Schubert et al. 2002) similar to that found here for the pan-Pacific pattern.

While there is a clear link between the Great Plains precipitation and the pan-Pacific SST pattern of variability, SST fluctuations account for only about one-third of the total low-frequency variability in the precipitation. The remaining two-thirds of the variability in the low-frequency Great Plains precipitation variability is internally generated. Results from a series of runs with climatological SSTs suggest that the low-frequency variations that occur in the absence of SST forcing require soil moisture feedback. In particular, simulations without soil moisture feedback show a fivefold decrease in the variance in annual Great Plains precipitation compared with simulations that include soil feedback. The interactions with the soil also introduce year-to-year memory in the hydrological cycle that is consistent with a red noise process, in which the deep soil is forced by white noise and damped with a time scale of about 1.5 yr. This suggests that at least part of the low-frequency behavior in the Great Plains precipitation is tied to the long-term memory inherent in the deep soil. We note that this is distinctly different from the

month-to-month memory in the precipitation (e.g., Koster et al. 2000), which is most affected by the faster time scales of atmospheric variability and the top layers of the soil.

While SSTs force a global-scale response in the height field that is generally consistent with the precipitation changes over the Great Plains (reduced heights during pluvial conditions and enhanced heights during drought conditions), the exact mechanism by which the precipitation is impacted (in terms of changes in the storm tracks, suppressed rising motion, and changes in moisture transport) has not been established. The seasonal cycle of the response to the idealized forcing (Figs. 8 and 9) suggests that the seasons and/or polarities of SST forcing with more zonally oriented height anomalies over the North Pacific–North American sector tend to be associated with the largest impacts on the Great Plains precipitation (cf., e.g., the results for the positive polarity of the forcing during DJF and MAM). This suggests that changes in the number or intensity of Pacific storms entering the continent (especially during the spring) may play a key role. An increase (decrease) in springtime storms would presumably also contribute to wet (dry) conditions during the following summer through the month-to-month persistence of soil moisture anomalies. Long-term drought in the Great Plains can therefore be viewed as occurring partly through the direct effect of long-term tropical SST variations through their impact on spring and summer precipitation (the former through changes in the number/intensity of storms, and the latter coming partly from month-to-month memory in the soil), and partly as a result of the deep soil acting as a long-term reserve for both forced and random warm season (primarily spring and summer) precipitation anomalies.

A related issue concerns the link between the effects of ENSO and the effects of the low-frequency pan-Pacific SST mode on the Great Plains precipitation. It is not clear, for example, why the model generates consistently dry conditions during the 1930s, but not during the 1950s when the pan-Pacific SST pattern has a sign and amplitude that is similar to that of the 1930s. In fact, the amplitude of the pan-Pacific pattern is not particularly large during the 1930s. One reason for the difference could be the differences in the character of ENSO. The 1930s were characterized by a distinct lack of ENSO activity, suggesting it is the combination of weak ENSO and negative values of the pan-Pacific SST pattern that is particularly conducive to drought in the U.S. Great Plains. As such, we might consider ENSO warm events to periodically recharge the soil water reservoir, to help avoid prolonged (multiyear) drought conditions. Understanding the role of ENSO in long-term drought requires that we better understand the relationship between ENSO and low-frequency SST variability (e.g., Zhang et al. 1997). It is noteworthy that the correlation patterns linking Great Plains precipitation to SST at the higher frequencies (the residual variability

with time scales less than 6 yr—not shown) are somewhat similar to those for the low frequencies shown in Fig. 3. The main differences are overall weaker correlations and a narrower (in latitude) region of positive SST correlations in the eastern tropical Pacific Ocean for the residual (ENSO) variability.

We see some intriguing evidence for decadal differences in the strength of the coupling between the SST and Great Plains precipitation—note the better agreement among the ensemble members and the observations in the last two decades (Fig. 1). A key issue is whether long-term variations in the basic state of the tropical oceans impacts the link with the Great Plains, or more generally with the midlatitudes. That this may be the case is suggested by Hoerling and Kumar (2003), who showed that the recent unprecedented warming of the tropical Indian and western Pacific Oceans and a concomitant cooling in the eastern tropical Pacific contributed to the widespread multiyear drought in the northern midlatitudes.

The results presented here are clearly model dependent. The scarcity of soil moisture (especially deep soil moisture) observations makes it difficult to verify the estimates of year-to-year soil memory. The NSIPP system tends to have a stronger land–atmosphere coupling than some other models (Koster et al. 2002). Assessing the model dependency will require comparisons with the results of other long simulations with several different models. Such runs are currently being carried out as part of the Climate of the Twentieth Century Project (WMO 2001).

Acknowledgments. We thank Mike Wallace and an anonymous reviewer for valuable comments and suggestions that helped to clarify several aspects of the results. This work was supported by the NASA Earth Science Enterprise's Global Modeling and Analysis Program, and the NASA Seasonal-to-Interannual Prediction Project.

REFERENCES

- Atlas, R., N. Wolfson, and J. Terry, 1993: The effect of SST and soil moisture anomalies on the GLA model simulations of the 1988 U.S. drought. *J. Climate*, **6**, 2034–2048.
- Bacmeister, J., P. J. Pegion, S. D. Schubert, and M. J. Suarez, 2000: An atlas of seasonal means simulated by the NSIPP 1 atmospheric GCM. Vol. 17. NASA Tech. Memo. 104606, Goddard Space Flight Center, Greenbelt, MD, 194 pp.
- Bark, D. L., 1978: History of American droughts. *North American Droughts*, N. J. Rosenberg, Ed., AAAA Selected Symposium Series, Vol. 15, Westview Press, 9–23.
- Barlow, M., S. Nigam, and E. H. Berbery, 2001: ENSO, Pacific decadal variability, and U.S. summertime precipitation, drought, and streamflow. *J. Climate*, **14**, 2105–2128.
- Beljaars, A. C. M., P. Viterbo, M. J. Miller, and A. K. Betts, 1996: The anomalous rainfall over the United States during July 1993: Sensitivity to land surface parameterization and soil moisture anomalies. *Mon. Wea. Rev.*, **124**, 362–383.
- Borchert, J. R., 1971: The dust bowl in the 1970's. *Assoc. Amer. Geogr. Ann.*, **61**, 1–22.

- Box, G. E. P., and G. M. Jenkins, 1976: *Time Series Analysis: Forecasting and Control*. Holden Day, 575 pp.
- Chang, F. C., and J. M. Wallace, 1987: Meteorological conditions during heat waves and droughts in the United States Great Plains. *Mon. Wea. Rev.*, **115**, 1253–1269.
- Charney, J. G., 1975: Dynamics of deserts and drought in the Sahel. *Quart. J. Roy. Meteor. Soc.*, **101**, 193–202.
- Chou, M.-D., and M. J. Suarez, 1994: An efficient thermal infrared radiation parameterization for use in general circulation models. Vol. 3. NASA Tech. Memo. 104606, NASA Goddard Space Flight Center, Greenbelt, MD, 85 pp.
- , and —, 2000: A solar radiation parameterization for atmospheric studies. Vol. 11. NASA Tech. Memo. 104606, NASA Goddard Space Flight Center, Greenbelt, MD, 40 pp.
- Dettinger, M. D., D. S. Battisti, G. J. McCabe, C. M. Bitz, and R. D. Garreaud, 2001: Interhemispheric effects of interannual and decadal ENSO-like climate variations on the Americas. *Interhemispheric Climate Linkages: Present and Past Climates in the Americas and Their Societal Effects*, V. Markgraf, Ed., Academic Press, 1–16.
- Felch, R. E., 1978: Drought: Characteristics and assessment. *North American Droughts*, N. J. Rosenberg, Ed., AAAA Selected Symposium Series, Vol. 15, Westview Press, 25–42.
- Hoerling, M. P., and A. Kumar, 2003: The perfect ocean for drought. *Science*, **299**, 691–699.
- Hughes, P., 1976: Drought: The land killer. *American Weather Stories*, U.S. Dept. of Commerce, NOAA-EDS, 77–87.
- Kalnay, E., and Coauthors, 1996: The NCEP/NCAR 40-Year Reanalysis Project. *Bull. Amer. Meteor. Soc.*, **77**, 437–471.
- Koster, R. D., and M. J. Suarez, 1996: Energy and water balance calculations in the Mosaic LSM. Vol. 9. NASA Tech. Memo. 104606, 194 pp.
- , —, and M. Heiser, 2000: Variance and predictability of precipitation at seasonal-to-interannual timescales. *J. Hydrometeor.*, **1**, 26–46.
- , P. A. Dirmeyer, A. N. Hahmann, R. Ijpelaar, L. Tyahla, P. Cox, and M. J. Suarez, 2002: Comparing the degree of land–atmosphere interaction in four atmospheric general circulation models. *J. Hydrometeor.*, **3**, 363–375.
- Livezey, R., and T. Smith, 1999: Covariability of aspects of North American climate with global sea surface temperatures on interannual to interdecadal timescales. *J. Climate*, **12**, 289–302.
- Louis, J., M. Tiedtke, and J. Geleyn, 1982: A short history of the PBL parameterization at ECMWF. *Proc. ECMWF Workshop on Planetary Boundary Layer Parameterization*, Reading, United Kingdom, ECMWF, 59–80.
- Lyon, B., and R. M. Dole, 1995: A diagnostic comparison of the 1980 and 1988 United States summer heat wave–droughts. *J. Climate*, **8**, 1658–1676.
- Mantua, N., S. Hare, Y. Zhang, J. M. Wallace, and R. Francis, 1997: A Pacific interdecadal climate oscillation with impacts on salmon production. *Bull. Amer. Meteor. Soc.*, **78**, 1069–1079.
- Mo, K. C., J. Noguez-Paegle, and R. W. Higgins, 1997: Atmospheric processes associated with summer floods and droughts in the central United States. *J. Climate*, **10**, 3028–3046.
- Moorthi, S., and M. J. Suarez, 1992: Relaxed Arakawa–Schubert: A parameterization of moist convection for general circulation models. *Mon. Wea. Rev.*, **120**, 978–1002.
- Namias, J., 1955: Some meteorological aspects of drought with special reference to the summers of 1952–1954 over the United States. *Mon. Wea. Rev.*, **83**, 199–205.
- , 1982: Anatomy of Great Plains protracted heat waves (especially the 1980 U.S. summer drought). *Mon. Wea. Rev.*, **110**, 824–838.
- Pegion, P. J., S. D. Schubert, and M. J. Suarez, 2000: An assessment of the predictability of northern winter seasonal means with the NSIPP 1 AGCM. Vol. 18. NASA Tech. Memo. 104606, Goddard Space Flight Center, Greenbelt, MD, 110 pp.
- Rayner, N. A., E. B. Horton, D. E. Parker, C. K. Folland, and R. B. Hackett, 1996: Version 2.2 of the Global Sea-Ice and Sea Surface Temperature dataset, 1903–1994. Met Office Climate Research Tech. Note 74, Hadley Centre, United Kingdom, 35 pp.
- , D. E. Parker, E. B. Horton, C. K. Folland, L. V. Alexander, D. P. Rowell, E. C. Kent, and A. Kaplan, 2003: Global analyses of sea surface temperature, sea ice and night marine air temperature since the late nineteenth century. *J. Geophys. Res.*, **108**, 4407, doi:10.1029/2002JD002670.
- Reynolds, W. R., and T. M. Smith, 1994: Improved global sea surface temperature analyses using optimum interpolation. *J. Climate*, **7**, 929–948.
- Ropelewski, C., and M. Halpert, 1986: North American precipitation and temperature patterns associated with El Niño/Southern Oscillation (ENSO). *Mon. Wea. Rev.*, **114**, 2352–2362.
- Rowell, D. P., C. Folland, K. Maskell, and N. Ward, 1995: Variability of summer rainfall over tropical North Africa (1906–92): Observations and modeling. *Quart. J. Roy. Meteor. Soc.*, **121**, 669–704.
- Schubert, S. D., M. J. Suarez, P. J. Pegion, M. A. Kistler, and A. Kumer, 2002: Predictability of zonal means during boreal summer. *J. Climate*, **15**, 420–434.
- Stuart, A., and J. K. Ord, 1994: *Kendall's Advanced Theory of Statistics*. Halsted Press, 676 pp.
- Suarez, M. J., and L. L. Takacs, 1995: Documentation of the Aries-GEOS dynamical core: Version 2. Vol. 5. NASA Tech. Memo. 104606, Goddard Space Flight Center, Greenbelt, MD, 45 pp.
- Ting, M., and H. Wang, 1997: Summertime U.S. precipitation variability and its relation to Pacific sea surface temperature. *J. Climate*, **10**, 1853–1873.
- Trenberth, K. E., and G. W. Branstator, 1992: Issues in establishing causes of the 1988 drought over North America. *J. Climate*, **5**, 159–172.
- , and C. J. Guillemot, 1996: Physical processes involved in the 1988 drought and 1993 floods in North America. *J. Climate*, **9**, 1288–1298.
- , G. W. Branstator, and P. A. Arkin, 1988: Origins of the 1988 North American drought. *Science*, **242**, 1640–1645.
- Vose, R., R. Schmoyer, P. Steurer, T. Peterson, R. Heim, T. Karl, and J. Eischeid, 1992: The Global Historical Climatology Network: Long-term monthly temperature, precipitation, sea level pressure, and station pressure data. Carbon Dioxide Information Analysis Center, Oak Ridge National Laboratory ORNL/CDIAC-53, NDP-041, Oak Ridge, TN, 296 pp.
- WMO, 2001: Report of the sixteenth session of the CAS/JSC working group on numerical experimentation. WMO-TD 1076, 42 pp.
- Woodhouse, C. A., and J. T. Overpeck, 1998: 2000 years of drought variability in the central United States. *Bull. Amer. Meteor. Soc.*, **79**, 2693–2714.
- Worster, D., 1979: *Dust Bowl: The Southern Great Plains in the 1930s*. Oxford University Press, 277 pp.
- Zhang, Y., J. M. Wallace, and D. Battisti, 1997: ENSO-like interdecadal variability: 1900–93. *J. Climate*, **10**, 1004–1020.